TRENDS IN SCIENCES 2026; 23(12): 13726
https://doi.org/10.48048/tis.2026.13726
RESEARCH ARTICLE

Swertiamarin Induces Cytotoxicity in KYSE-150 Esophageal Squamous Cell Carcinoma Cells with Potential to Target Multiple Cell Death Pathways

Yan Mei Chong[1], Fook Choy Yap[1], Bibi Ghausia Banon Aullyram[1], Mahendran Sekar[2], Sang Loon Tan[3] and Yuan Seng Wu[1,4,*]

[1]Department of Biomedical Sciences, Jeffery Cheah Sunway Medical School, Faculty of Medical and Life Sciences, Sunway University, Sunway, Malaysia
[2]School of Pharmacy, Monash University Malaysia, Selangor, Malaysia
[3]Sunway Biofunctional Molecules Discovery Centre, Faculty of Medical and Life Sciences, Sunway University, Sunway, Malaysia
[4]Sunway Microbiome Centre, Faculty of Medical and Life Sciences, Sunway University, Sunway, Malaysia

([*]Corresponding author's e-mail: yuansengw@sunway.edu.my)

Received: 4 March 2026, Revised: 9 May 2026, Accepted: 19 May 2026, Published: 10 July 2026

Abstract

Esophageal squamous cell carcinoma (ESCC) is an aggressive malignancy with poor chemotherapy outcomes, necessitating safer and more effective anticancer agents. Swertiamarin (STM), a natural compound, demonstrates anticancer potential, but its cytotoxicity and associated molecular mechanisms in ESCC remain unclear. To evaluate STM's drug-likeness, cytotoxicity, and molecular mechanisms in ESCC using *in vitro* and *in silico* approaches. STM's physicochemical properties, pharmacokinetics, and toxicity profile were predicted via SwissADME and ProTox 3.0. Cytotoxicity was assessed by MTT assay in ESCC KYSE-150 cells and 2 normal cell lines (HET-1A and Vero), alongside cisplatin and 5-fluorouracil (5-FU) as controls. Molecular docking was used to predict STM's binding affinities with proteins involved in apoptosis, necroptosis, ferroptosis, and pyroptosis. STM showed a favorable drug-likeness and predicted class 4 toxicity. It exhibited the concentration-dependent cytotoxicity with half-maximal inhibitory concentration (IC_{50}) values of 43.75 µM (KYSE-150 cells), 190 µM (HET-1A cells), and 41.61 µM (Vero cells), causing selectivity indices (SI) of 4.343 (HET-1A/KYSE-150) and 0.951 (Vero/KYSE-150), outperforming cisplatin (SI = 0.668). Docking revealed strong binding to key proteins, notably pro-apoptotic APAF-1 (−12.3 kcal/mol), anti-ferroptotic FSP1 (−12.1 kcal/mol), anti-apoptotic Hsp70 (−11 kcal/mol), and necroptotic MLKL (−10.8 kcal/mol). Detailed topological analysis with APAF-1 and FSP1 confirmed stable interactions via hydrogen and hydrophobic bonds. STM demonstrates promising cytotoxicity and selectivity against KYSE-150 cells and targets multiple cell death pathways, supporting its potential as a candidate for ESCC chemotherapy and deserve further preclinical investigations.

Keywords: Swertiamarin, Esophageal squamous cell carcinoma, Cytotoxicity, Selectivity index, Molecular mechanism, Molecular docking, Multi-death pathway targets

Introduction

Esophageal cancer is a highly aggressive malignancy with a disproportionately high mortality rate, accounting for approximately 600,000 global diagnoses annually [1,2]. Esophageal squamous cell carcinoma (ESCC) is the most prevalent subtype, representing 90% of worldwide cases, primarily concentrated in Asia and South Africa [3-7]. ESCC pathogenesis involves a multistep progression driven by the interaction of environmental exposures and molecular alterations. The major risk of complexity in ESCC is mainly influenced by lifestyle factors such as tobacco use and excessive alcohol consumption. At the molecular level, ESCC is often associated with the

dysregulations of key regulatory genes like *TP53*, *NOTCH1*, and *PIK3CA* [8-11]. The prognosis of ESCC remains poor, with 5-year survival rates dropping to only 5% for distant metastatic disease [12]. This unfavorable outcome is driven by rapid recurrence, metastasis, and the clinical limitations of current therapeutic strategies [13]. While localized ESCC may be managed through endoscopic resection or radiochemotherapy, palliative chemotherapy remains the standard of care for advanced cases. To date, cisplatin and 5-fluorouracil (5-FU) continue to serve as the first-line chemotherapeutic agents for ESCC [14].

Despite being the first-line treatment for advanced ESCC, cisplatin and 5-FU encounter several limitations. Their cytotoxic mechanisms lack specificity, leading to dose-limiting toxicities in healthy cells and organs. This includes nephrotoxicity, ototoxicity, and myelosuppression from cisplatin, and liver, kidney, lung, and neurological toxicities from 5-FU [15-17]. Furthermore, the development of resistance in cancer cells also obstructs their efficacy. Cancer cells have developed the ability to reduce drug entry by reducing transporters and channels on the cell surface, employing DNA repair mechanisms, and altering gene expression and intracellular signaling pathway to inhibit cytotoxicity [18,19]. These challenges contribute to the modest 20% - 50% response rates of combination therapy in ESCC patients, therefore leading to greater risk of recurrence and metastasis, and ultimately, poor prognosis [14,20]. Considering these challenges, there is an urgent need to develop more effective and selective therapeutic agents.

Naturally occurring, seco-iridoid glycosides such as swertiamarin (STM) have been intensively researched for its abundant occurrence in medicinal plants and its various pharmacological properties. STM can be obtained from plants of the Gentianaceae family, particularly from the genus *Enicostemma*. This glycoside has been reported to possess numerous properties including analgesic, anti-inflammatory, antioxidant, and anticancer [21]. It has exerted great *in vitro* anticancer activity against human cancer cells, such as cervical (HeLa), lung (A549), and liver (HepG2, Huh7) [22-24]. Its anticancer properties are also reflected in hepatic injuries-induced mice [24-26]. Current research also suggests STM's role in modulating signaling pathways such as the FRAT1/Wnt/β-catenin signaling axis, MEK/ERK, and PI3K/Akt/GSK3β signaling pathways, as well as altering the expression of proteins such as caspases and apoptotic proteins to exert its properties [21,24,27,28]. Despite increasing evidence of STM's anticancer potential, its effects and molecular mechanisms in ESCC remain largely unexplored.

This study aimed to investigate the STM's potential as a chemotherapeutic agent against ESCC by evaluating its drug-likeness and cytotoxicity effects. Moreover, molecular docking was utilized to understand the potential cell death mechanisms targeted by STM.

Materials and methods

Chemicals

5-FU was purchased from MACKLIN (Shanghai, China). Cisplatin was purchased from BOMEi Co., Ltd. (Taiwan).3-(4,5-dimethylthiazol-2-yl)-2,5 diphenyltetrazolium bromide (MTT) and swertiamarin (STM) were purchased from Merck (New Jersey, USA).

Cell culture

Normal esophageal epithelial cell line (HET-1A) (iCell Bioscience iCell-h333, Shanghai, China; RRID:CVCL 3702), ESCC cell line (KYSE-150) (iCell Bioscience iCell-h245, Shanghai, China; RRID: CVCL_1348), and normal monkey kidney epithelial cell line (Vero) (ATCC CCL-81, USA; RRID:CVCL_0059) were used in this study. Briefly, HET-1A and Vero cells were cultured in Dulbecco's Modified Eagle Medium (DMEM) (Nacalai Tesque, Kyoto, Japan) supplemented with 10% fetal bovine serum (FBS) (Gibco, USA) and 1% penicillin-streptomycin (Pen/Step) (Gibco, USA). KYSE-150 cells were cultured in RPMI-1640 medium (Nacalai Tesque, Kyoto, Japan) supplemented with 10% FBS (Gibco, USA) and 1% Pen/Strep (Gibco, USA).

Drug preparation

STM stock solution (0.1 M) was prepared in dimethyl sulfoxide (DMSO). For KYSE-150 cell treatment, a working solution (400 µM) was prepared in RPMI-1640 complete media. Two-fold serial dilutions were performed to achieve concentrations of 1.5625, 3.125, 6.25, 12.5, 25, 50, 100, 200, and 400 µM. The stock solution of 5-FU (0.1 M) was prepared using distilled water, and a 200 µM working solution was further prepared in RPMI-1640 complete media. While for cisplatin, a 3.33 mM stock solution was prepared in

distilled water, and a 200 μM working solution was prepared in RPMI-1640 complete media. Two-fold serial dilutions of 5-FU and cisplatin were then performed to achieve concentrations of 1.5625, 3.125, 6.25, 12.5, 25, 50, 100 and 200 μM. The working concentrations of STM, 5-FU, and cisplatin were then used for treating KYSE-150, HET-1A, and Vero cells. In all experiments, the final concentration of DMSO in the highest drug concentration did not exceed 1% (v/v) to avoid solvent-induced cytotoxicity.

MTT cytotoxicity assay

The *in vitro* cytotoxicity of STM was investigated in KYSE-150, HET-1A, and Vero cells. Cells were seeded into 96-well cell culture plates at a seeding density of 2×10^4 cells/well in their respective complete growth media and incubated for 24 h at 37 °C in an 5% CO_2 incubator. Following incubation, cells were then treated with the prepared drug concentrations in their respective wells and incubated for an additional 24 h. After the treatment period, 20 μL of MTT solution were added into each well, and the plates were incubated in the dark for 2 h at 37 °C with 5% CO_2. Next, 100 μL of 10% sodium dodecyl sulfate (SDS) (Bio-Rad Laboratories, Inc., USA)/0.01 M hydrochloric acid (HCl) were added into each well and incubated for 24 h at 37 °C with 5% CO_2. Lastly, the absorbance was measured at 570 nm with a reference wavelength of 630 nm by Tecan Infinite MPro multiplate reader (Tecan, Männedorf, Switzerland). The obtained absorbance was used to calculate the cell viability using the formula followed:

$$\text{Cell viability (\%)} = \frac{\text{Absorbance of treated well} - \text{Absorbance of blank well}}{\text{Absorbance of negative control well} - \text{Absorbance of blank well}} \times 100\%$$

The selectivity index (SI) of STM was calculated using the formula below:

$$\text{SI} = \frac{\text{IC50,normal cells}}{\text{IC50,cancer cells}}$$

Drug-likeness screening and toxicity prediction

The SMILES code of STM (C=C[C@H]1[C@@H](OC=C$_2$[C@]1(CCOC$_2$=O)O)O[C@H]$_3$[C@@H]([C@H]([C@@H]([C@H](O$_3$)CO)O)O)O) was used to predict the physicochemical properties, pharmacokinetics, and drug-likeness using the SwissADME webtool (SwissDrugDesign). STM's toxicity was also predicted with the virtual toxicity lab ProTox 3.0.

Selection and preparation of ligand and target proteins

Target protein 3D structures were obtained from Research Collaboratory for Structural Bioinformatics Protein Data Bank (PDB), with selection criteria focusing on proteins known to be actively involved in investigated cell death pathways of apoptosis, ferroptosis, necroptosis, and pyroptosis. A comprehensive list of the selected proteins and their corresponding PDB codes is shown in **Table 1**. The proteins were prepared by removing non-standard residues and isolating the target polypeptide chain using University of California, San Francisco Chimera (UCSF Chimera) v1.19 [29]. STM's 3D conformer was obtained from PubChem of the National Library of Medicine in Structure Data File (SDF) format and chemically converted to PDB format using Open Babel v3.1.0. The structures of both prepared proteins and ligand were then imported into AutoDockTools (ADT) v1.5.7 for addition of hydrogens and computation of Gasteiger charges. The modified structures were saved as Protein Data Bank, Partial Charge, and Atom Type (PDBQT) files. Then, the predicted active site coordinates of each modified protein structure were obtained using the PrankWeb server by P2Rank.

Table 1 Selected target proteins in various cell death pathways and their PDB codes.

Target Proteins	**PDB Code**
Anti-Apoptotic	
B-cell lymphoma-extra-large, BCL-XL	7LH7
Myeloid cell leukemia 1 protein, MCL-1	5FDR
Apoptosis regulator, BCL-W	4K5A
BCL-2-like protein 10, BCL2L10	4B4S

Target Proteins	PDB Code
Anti-Apoptotic	
BCL-2-related protein A1, A1/Bfl-1	2VM6
Heat shock protein 70, Hsp70	3ATU
Heat shock protein 90, Hsp90	2XJX
Pro-Apoptotic	
Caspase-9	1JXQ
Apoptotic protease activating factor 1, APAF-1	1Z6T
Caspase-3	2CNN
Pro-apoptotic BIM BH3 peptide	2WH6
Human cytochrome c	3ZCF
BCL-2/adenovirus E1B interacting protein 3, BNIP3	4IEH
Pro-apoptotic BID peptide	7M5A
Apoptosis regulator, BAX	4ZIE
Second mitochondria-derived activator of caspase/direct inhibitor of apoptosis-binding protein with low pI, SMAC/DIABLO	1FEW
BCL-2 homologous antagonist/killer, BAK	2YV6
Activator of apoptosis Harakiri, Hrk	6XY4
Tumor necrosis factor receptor, TNFR	1NCF
Tumor necrosis factor-related apoptosis-inducing ligand receptor, TRAIL	1D4V
Apoptosis-mediating surface antigen FAS	3TJE
FAS-associated death domain, FADD	3EZQ
TNFR1-associated death domain protein, TRADD	1F3V
Caspase-7	1K86
Caspase-8	1I4E
Tumor protein p53	4MZI
Anti-Ferroptotic	
Ferroptosis suppressor protein 1, FSP1 OR Apoptosis-Inducing Factor, Mitochondrion-Associated 2, AIFM2	8JSC
Necroptosis-Related	
Tumor necrosis factor alpha, TNFα	1A8M
Receptor-interacting serine/threonine-protein kinase 1, RIPK1	4ITH
Receptor-interacting serine/threonine-protein kinase 3, RIPK3	7MON
Mixed lineage kinase domain like pseudokinase, MLKL	4M67
Dynamin-related protein 1 (Drp1) OR dynamin-1-like protein (DNM1L)	3W6N
Pyroptosis-Related	
Interferon-inducible protein, AIM2 (Absent in melanoma 2)	3RN2
Pyrin	4CG4
Caspase-1	2FQQ
Gasdermin D, GSDMD	6N9O
Interleukin IL-1β	1I1B

Molecular docking and validation

Molecular docking was performed using AutoDockVina v1.2.7. Input prompts were prepared for each modified protein, including the PDBQT files of proteins and ligand, predicted active site coordinates, exhaustiveness, and energy range. The binding affinity of energy (kcal/mol) from the best predicted pose was recorded for each complex. The topology interactions of STM with the 2 strongest binding proteins were then illustrated with BIOVIA Discovery Studio Visualiser 2025 by Dassault Systèmes [30] and UCSF Chimera v1.19.

The protocol was validated by re-docking known ligands with the target protein structures. Protein structures with co-crystallized ligands were obtained from PDB. Individual protein chains and their known ligand were isolated and prepared using UCSF Chimera v1.19 and AutoDockTools (ADT) v1.5.7. The active site coordinates were predicted and obtained using the PrankWeb server by P2Rank. Re-docking was performed using AutoDockVina v1.2.7. The best predicted ligand pose was then superimposed onto the experimental co-crystallized structures in UCSF Chimera v1.19 for structural comparison. Re-docking was considered valid if the Root Mean Square Deviation (RMSD) value was less than 1.00 Å.

Statistical analysis

All experiments were conducted in triplicates in 3 independent biological replicates. GraphPad Prism v10.4.2 (GraphPad Software, USA) was used to determine the IC_{50} values, perform statistical analysis, and generate graphical illustrations. Data were expressed as mean (standard deviation [SD]). Normality of the data was assessed using Shapiro-Wilk test, and the homogeneity of variance was confirmed via the Brown-Forsythe test ($p > 0.05$), justifying the use of ordinary One-way ANOVA. Subsequent multiple comparisons between the negative control and treated groups were performed using Dunnett's post-hoc test. Statistical significance was defined as $p < 0.05$ and assigned to values with an asterisk (*).

Results and discussion

In vitro cytotoxic patterns of STM against KYSE-150, HET-1A, and Vero cells

STM exhibited a notable concentration-dependent cytotoxic pattern toward KYSE-150, HET-1A, and Vero cells, as seen in the gradual decrease in cell viability as the tested concentrations increased (**Figure 1**). For instance, there was a more pronounced decrease in viability when concentration is more than 50 µM. Cell viability of KYSE-150 dropped from 100% at 0 µM to 35% at 400 µM. Over the same concentration range, STM induced a greater degree of reduction in KYSE-150 cell viability as compared to HET-1A (44%) and Vero (48%) cells for all the test concentrations, particularly 100 to 400 µM.

The IC_{50} values of STM were determined to be 43.75 µM for KYSE-150, 190 µM for HET-1A, and 41.61 µM for Vero cells. These findings indicate that STM exerts its cytotoxicity effects in a concentration-dependent manner, consistent with recent studies on its efficacy in other cancer cell lines, such as hepatocellular carcinoma (Huh7 and HepG2) [31] and cervical cancer (HeLa) [22]. When compared with other natural compounds such as curcumin (IC_{50} = 15 µM) [32], decursin (IC_{50} = 14.62 µM) [33], and carnosic acid (IC_{50} = 29.87 µM) [34], STM appears to have better therapeutic potential against KYSE-150 cells based on its SI value. Moreover, STM demonstrated a better safety margin, with an SI of 4.34, compared with decursin, which showed a minimum SI of 1.09 against HET-1A/KYSE-150 [33]. Although carnosic acid has been shown to be highly potent, it only demonstrates a broad safety profile against normal liver cells (MIHA), with an SI of 6.70 [34]. In contrast, STM's selectivity is specifically directed toward esophageal cells, indicating its potential as a more targeted anti-ESCC agent.

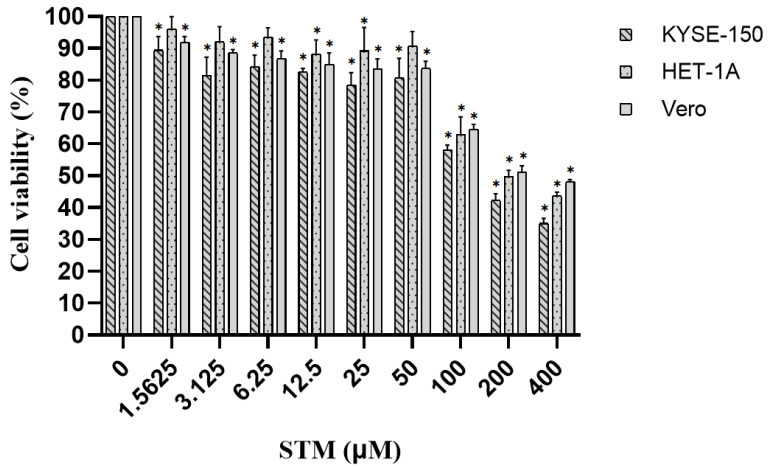


Figure 1 Percentage of KYSE-150, HET-1A, Vero cell viability after STM treatment as measured by MTT assay. Error bars indicate the mean ± SD of the 3 replicates conducted, with statistical significance analysed by one-way ANOVA and Dunnett's test and indicated as (*$p < 0.05$) when compared with the control group (0 μM).

***In vitro* cytotoxic patterns of 5-FU against KYSE-150, HET-1A, and Vero cells**

Next, the cytotoxicity of 5-FU (**Figure 2**), which is one of the positive control drugs, was also evaluated. At the highest concentration of 200 μM, cell viability decreased to 61% for KYSE-150, 72% for HET-1A, and 56% for Vero cells, from the initial 100% cell viability at 0 μM. This showed that 5-FU induced the greatest cytotoxicity in Vero cells, while the KYSE-150 and HET-1A cells were relatively less sensitive toward 5-FU. Its cytotoxic pattern was concentration-dependent, though its IC_{50} remained undetermined, indicating a value greater than 200 μM. This finding is opposed to numerous studies, which have reported that IC_{50} values for 5-FU against KYSE-150 cells range from 4 to 36.87 μM [35-37], 20 to 160 μM in HET-1A cells [38], and more than 700 μM in Vero cells [39]. The variation in cytotoxic performance compared to existing findings may be due to differences in experimental conditions, including media used, treatment duration, cell seeding density, or even cell line passage number [40-43].

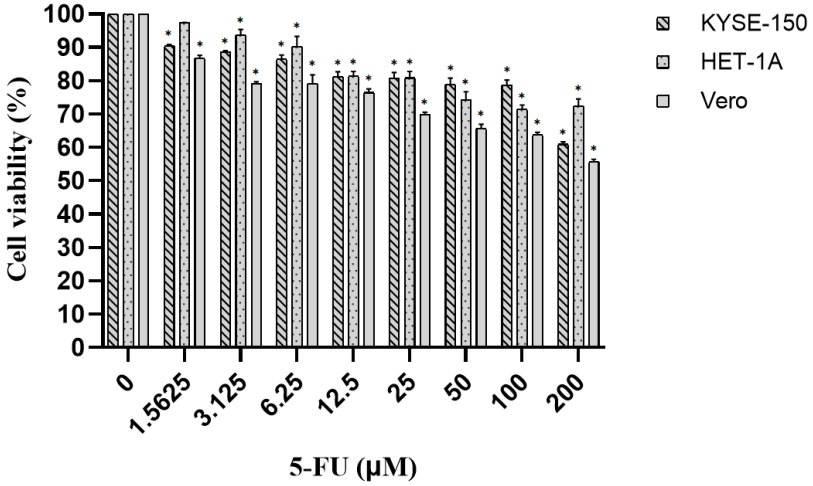


Figure 2 Percentage of KYSE-150, HET-1A, and Vero cell viability after 5-FU treatment as measured by MTT assay. Error bar**s** represent the mean ± SD between the triplicates of the data. Statistical significance performed by one-way ANOVA and Dunnett's test were indicated to each value as * ($p < 0.05$) when compared with the control group (0 μM).

***In vitro* cytotoxic patterns of cisplatin against KYSE-150, HET-1A, and Vero cells**

The cytotoxic effect of cisplatin demonstrated a lower IC_{50} against all 3 cell lines compared to STM (**Figure 3**). However, the determined IC_{50} of 36.46 μM against KYSE-150 suggests cisplatin to be moderately potent in general *in vitro* anticancer screening. Moreover, the demonstrated greater cytotoxic effects on the normal HET-1A (IC_{50} = 24.37 μM) and Vero cells (IC_{50} = 14.07 μM) indicated cisplatin's lack of tumor specificity. These findings are supported by literature, with reported IC_{50} value of cisplatin against KYSE-150 as 40.62 ± 1.13 μM by Wu *et al.* [44], while Muralisankar *et al.* [45] suggested 33.7 μM as the IC_{50} of cisplatin for Vero cells, aligning with our results. This lack of selectivity of cisplatin is a well and well-known limitation in clinical applications, often associated with severe systemic toxicity [46].

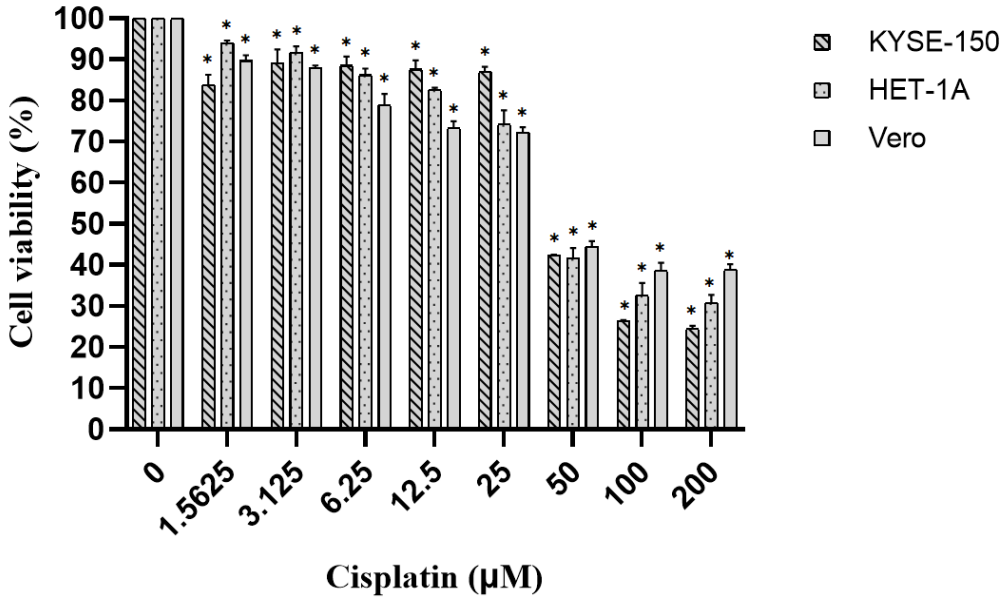


Figure 3 Percentage of KYSE-150, HET-1A, and Vero cell viability after cisplatin treatment as measured by MTT assay. Error bars are included to represent the SD between the data from 3 replicates, and statistical significance were analyzed using one-way ANOVA and Dunnett's test (*$p < 0.05$) when compared with the control group (0 μM).

Drug-likeness screening of STM

The *in-silico* drug-likeness and ADMET predictions provide crucial insights into STM's potential as an effective drug candidate. The analysis (**Figure 4**) revealed STM's desirable physicochemical properties with a Log $P_{o/w}$ value of −2.00, indicating acceptable lipophilicity (−0.7 < XLOGP3 < +5.0) and favorable molecular weight of 374.34 g/mol. Additionally, its fraction of sp3 hybridized carbons of 0.69 and 4 rotatable bonds indicated favorable saturation and flexibility. The predicted water solubility was generally acceptable, with a value of Log *S* (ESOL) of −0.64 (−6 < Log *S* (ESOL) < 0). The pharmacokinetics of STM were largely satisfactory, with inactiveness as a P-glycoprotein substrate and cytochrome (CYP) enzymes inhibitor, and impermeability of the blood-brain barrier (BBB), which suggests a reduced risk of drug-drug interactions [47]. Overall, STM's properties of molecular weight of 374.34 g/mol, octanol-water partition coefficient (Log *P*) at 1.66, 10 hydrogen bond acceptors, and 5 hydrogen bond donors adhered to Lipinski's Rule of Five, showing no violation. This adherence initially suggests that STM possesses satisfactory physicochemical parameters necessary for desirable ADME performance [48], positioning it as a promising candidate for an orally administered drug. However, its high-water solubility characterized by water partition coefficient (WLOGP) of –2.64 and high polarity evidenced by the topological polar surface area (TPSA) of 155.14 Å² resulted in violations of more stringent drug-likeness filters, including Ghose's, Veber's, Egan's, and Muegge's Rules. The high content of polar groups in STM stimulates aqueous solubility but consequently requires high desolvation energy,

which severely disrupts movement into and across the hydrophobic cell membranes. This limitation is supported by the predicted low gastrointestinal absorption, which contributed to a low bioavailability score of 0.11, indicating a potential challenge for oral administration [49]. This discrepancy accentuates the differing philosophies of drug-likeness assessment. While Lipinski's Rule of Five primarily limits the Log *P*, and the number of hydrogen bond acceptors and donors to restrict high energetic cost for efficient passive membrane permeation [50], rules proposed by Veber [51], Egan [52], and Muegge [53] cap the maximum TPSA to limit the number of polar groups. Therefore, the optimal drug delivery mechanism of STM should be explored. For instance, engineered nanoparticles and self-emulsifying drug delivery systems could potentially enhance STM's potency and efficacy by overcoming its barriers of low gastrointestinal absorption, poor oral bioavailability, and high hydrophilicity [54-56].

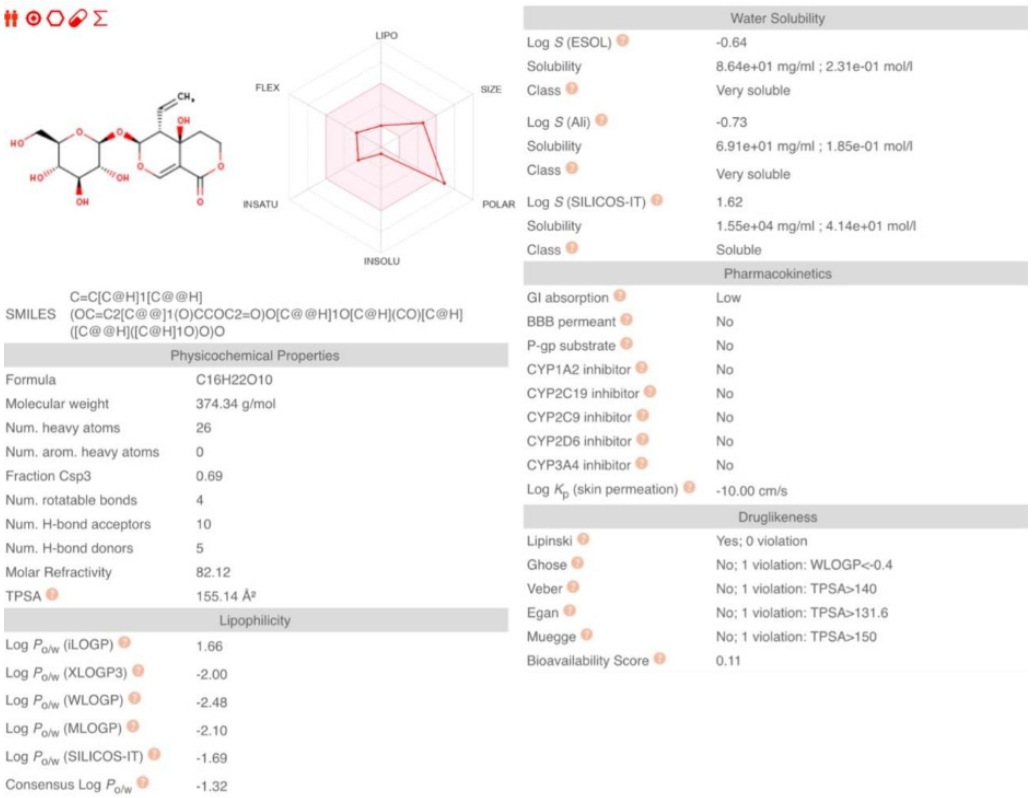


Figure 4 *In silico* pharmacological properties of STM consist of physicochemical properties, lipophilicity, water solubility, pharmacokinetics, and drug-likeness.

Toxicity prediction of STM

The results of toxicity prediction from ProTox 3.0 shown in **Figure 5** classified STM as a Class 4 compound defined by Globally Harmonized System of Classification and Labeling of Chemicals (GHS) as harmful if swallowed [57], with a predicted median lethal dose (LD_{50}) of 2,000 mg/kg, distinguished as slightly toxic [58]. The toxicological prediction exhibits great reliability as shown by the 100% average similarity and prediction accuracy, stemming from the direct comparison of STM against identical or near-identical analogue within the reference database. As summarized in **Table 2**, STM is unlikely to cause general cytotoxic effects, including hepatotoxicity, neurotoxicity, respiratory toxicity, carcinogenicity, immunotoxicity, and mutagenicity. Its inactiveness toward major drug-metabolizing CYP enzymes was also predicted. Nonetheless, it was speculated to be active for toxicity endpoints of BBB, nutritional toxicity, and clinical toxicity. This prediction shows a discrepancy regarding the BBB permeation, where toxicity prediction suggested potential BBB crossing, while pharmacokinetics evaluation predicted it to be non-permeant. The latter is further supported by Yang [28],

who reported STM's limited BBB permeability due to its high hydrophilicity. This observation highlights a limitation of *in silico* predictive models, where different algorithms can yield conflicting results, emphasizing the need for experimental validation [59]. ProTox 3.0 employs machine learning models trained on real toxicity datasets to predict the potential biological toxicity endpoints [60], while SwissADME applies rule-based methods and physicochemical descriptors to assess the pharmacokinetics and drug-likeness of compounds [61]. Due to their different approaches, predictive outputs should be interpreted cautiously.

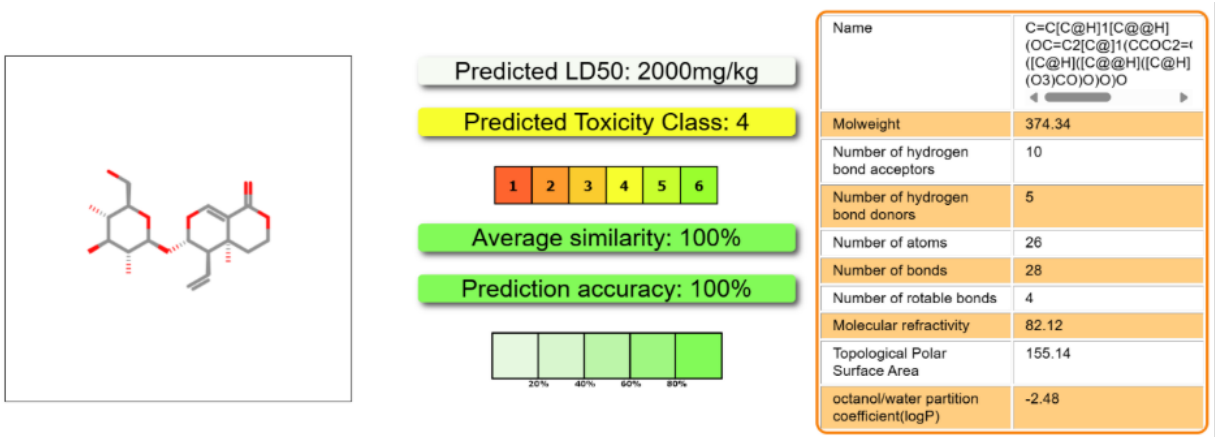


Figure 5 *In silico* toxicity prediction profile of STM highlighting a predicted LD_{50} of 2,000 mg/kg and a predicted toxicity of class 4. This profile includes key molecular descriptors and a 100% prediction accuracy based on similarity-based machine learning models.

Table 2 Toxicity profile detailed predicted activity of STM on organ toxicity, toxicity end points, and metabolism targets.

Classification	Target	Predicted Activity
Organ toxicity	Hepatotoxicity	Inactive
	Neurotoxicity	Inactive
	Nephrotoxicity	Active
	Respiratory toxicity	Inactive
	Cardiotoxicity	Active
Toxicity end points	Carcinogenicity	Inactive
	Immunotoxicity	Inactive
	Mutagenicity	Inactive
	Cytotoxicity	Inactive
	BBB-barrier	Active
	Clinical toxicity	Active
	Nutritional toxicity	Active
Metabolism	Cytochrome CYP1A2	Inactive
	Cytochrome CYP2C19	Inactive
	Cytochrome CYP2C9	Inactive
	Cytochrome CYP2D6	Inactive
	Cytochrome CYP3A4	Inactive
	Cytochrome CYP2E1	Inactive

Overall cytotoxicity and selectivity profiles of STM, 5-FU, and cisplatin

Table 3 shows the respective IC_{50} of STM, 5-FU, and cisplatin against KYSE-150, HET-1A, and Vero cells after 24 hours-treatment period. STM exhibited higher IC_{50} values across all 3 cell lines compared to cisplatin. Conversely, the IC_{50} for 5-FU exceeded the maximum tested concentration (200 μM) in all cell lines, suggesting that STM possesses greater cytotoxic potency than 5-FU under these experimental conditions**.** The therapeutic advantage of STM was also clearly reflected by its superior SI, a measure of a compound's ability to selectively target cancer cells over normal cells [62]. A value greater than 3 indicates high selectivity [63]. STM's SI value of 4.343 against HET-1A highlights its highly selective cytotoxicity toward ESCC cells over normal esophageal cells, where a wide therapeutic window allows maximum efficacy with minimized risk of adverse effects [64]. In contrast, cisplatin showed lower SI values of 0.668 for HET-1A/KYSE-150 and 0.386 for Vero/KYSE-150. This low SI indicates that cisplatin has less selectivity toward cancer cells, posing a risk of inducing cytotoxicity in normal cells. The difference in STM's selectivity between HET-1A and Vero cells suggests that a variety of toxicity profiles can exist for different tissue types and species, as supported by the toxicity prediction results (**Figure 2**).

The observed resistance of KYSE-150 cells to 5-FU (IC_{50} > 200 μM) aligns with previous reports of chemoresistance in esophageal squamous cell carcinoma (ESCC). This phenomenon is primarily attributed to altered gene expression, including the upregulation of *PFKFB3* and various long noncoding RNAs, which dysregulate metabolic pathways and increase the activity of catabolic enzymes such as dihydropyrimidine dehydrogenase (DPD) [37,65,66]. Furthermore, the relative insensitivity of Vero and HET-1A lines likely reflects 5-FU's characterization as a cell-cycle-specific antimetabolite. Given that 5-FU predominantly targets G1/S and S phases in rapidly dividing cells, its cytotoxic effect is commonly minimized in normal, healthy epithelial cells with slower doubling times [67,68], in which the 48-hour incubation period and optimized seeding densities utilized in this study may prevent the maximal inhibitory potential of 5-FU.

The implications of these findings extend to the clinical challenge of recurrent ESCC. Recurrent disease is frequently characterized by the selection of highly resistant cell subpopulations following initial rounds of chemotherapy, leading to treatment failure [69]. In this context, the significant cytotoxic effect of STM against the KYSE-150 cell model, which exhibits inherent 5-FU resistance [36], is particularly noteworthy and suggests its potential for the clinical treatment of recurrent ESCC. However, further investigations using more representative preclinical models and well-designed clinical studies are required to substantiate this claim.

Table 3 IC_{50} values (μM) of STM, 5-FU, and cisplatin in KYSE-150, HET-1A, and Vero cells obtained from MTT assay and SI of STM, 5-FU and cisplatin calculated using IC_{50} values (μM) of KYSE-150 based on HET-1A and Vero cells.

Compounds	IC_{50} values (μM)			SI values	
	ESCC Cell Line	Normal Cell Lines			
	KYSE-150	HET-1A	Vero	HET-1A	Vero
STM	43.75	190	41.61	4.343	0.951
Cisplatin	36.46	24.37	14.07	0.668	0.386
5-FU	> 200	> 200	> 200	Undetermined	Undetermined

Note: SI for 5-FU were not calculated due to undetermined IC_{50} (> 200 μM).

***In silico* molecular interactions of STM with selected target proteins**

This study further utilized *in silico* molecular docking to uncover STM's possible cell death mechanisms with promising results suggesting potential favorable cytotoxicity toward ESCC. STM exhibited strong binding affinities to a wide array of proteins involved in distinct cell survival and death pathways, including apoptosis, ferroptosis, necroptosis, and pyroptosis. Overall, the binding affinity energies of

STM toward the selected target proteins ranged from −7 to –12 kcal/mol.

Apoptosis pathway

Apoptosis is an important biological process that enables cells to undergo programmed cell death, allowing them to progress with normal development or response to external stress, yet it is often dysregulated by the cancer pathogenesis [70]. The extrinsic and intrinsic apoptotic pathways are orchestrated by the pro-apoptotic and pro-survival proteins in response to pro-apoptotic stimuli or intracellular activities [71]. STM showed exceptional binding to several anti-apoptotic proteins, including Hsp70, BCL-XL, and MCL-1 (**Table 4**). Given that BCL-XL and MCL-1 are pro-survival members of the BCL-2 protein family [72], and Hsp70 inhibits mitochondrial outer membrane permeabilization (MOMP) [73], the strong binding affinity of STM to their active sites (conventional hydrogen bonds: THR A:14, TYR A:15, GLY A:202; carbon hydrogen bonds: THR A:13, TYR A:15, SER A:340; pi-alkyl bond: TYR A:15) could indicate a potential inhibitory effect on these proteins. This antagonism of pro-survival cascades may inhibit cell proliferation or survival, aligning with the regulatory role of STM on c PI3K/AKT cell survival signaling as previously described by Zhang *et al.* [26].

As shown in **Table 5**, STM also exhibited strong binding affinities toward several pro-apoptotic proteins, with the highest affinity observed with APAF-1 (−12.3 kcal/mol), a key molecule in the intrinsic apoptosis pathway [74]. This interaction involved conventional hydrogen bonds (GLY D:157, LYS D:160, SER D:161, ASP D:243, and ARG D:265), carbon-hydrogen bonds (ASP D:243 and ASP D:392) and hydrophobic interactions (ALA D:156, PHE D:425, TYR D:436, and HIS D:438). Strong binding affinity energies were also observed with BID (−9.7 kcal/mol), BAX (−8.6 kcal/mol), and BAK (−7.3 kcal/mol), which are the main players in MOMP [72]. The significant interactions with these proteins, as well as with pro-apoptotic caspases, specifically caspase-7 and caspase-3 (**Table 5**), suggest that STM may modulate or facilitate their functions to promote apoptosis in cancer cells [75].

Table 4 Binding affinity energies of STM resulted from the *in silico* molecular docking toward corresponding anti-apoptotic proteins in ESCC.

Target Proteins	**PDB Code**	**Binding Affinity Energy (kcal/mol)**
Anti-Apoptotic		
B-cell lymphoma-extra-large, BCL-XL	7LH7	−10.4
Myeloid cell leukemia 1 protein, MCL-1	5FDR	−9.4
Apoptosis regulator, BCL-W	4K5A	−8.1
BCL-2-like protein 10, BCL2L10	4B4S	−9.0
BCL-2-related protein A1, A1/Bfl-1	2VM6	−8.2
Heat shock protein 70, Hsp70	3ATU	−11.0
Heat shock protein 90, Hsp90	2XJX	−9.0

Table 5 Binding affinity energies of STM toward the corresponding pro-apoptotic proteins as indicated in *in silico* molecular docking.

Target Proteins	**PDB Code**	**Binding Affinity Energy (kcal/mol)**
Pro-Apoptotic		
Caspase-9	1JXQ	−8.7
Apoptotic protease activating factor 1, APAF-1	1Z6T	−12.3
Caspase-3	2CNN	−9.4

Target Proteins **Pro-Apoptotic**	PDB Code	Binding Affinity Energy (kcal/mol)
Pro-apoptotic BIM BH3 peptide	2WH6	−8.3
Human cytochrome c	3ZCF	−8.8
BCL-2/adenovirus E1B interacting protein 3, BNIP3	4IEH	−9.1
Pro-apoptotic BID peptide	7M5A	−9.7
Apoptosis regulator, BAX	4ZIE	−8.6
Second mitochondria-derived activator of caspase/direct inhibitor of apoptosis-binding protein with low pI, SMAC/DIABLO	1FEW	−7.1
BCL-2 homologous antagonist/killer, BAK	2YV6	−7.3
Activator of apoptosis Harakiri, Hrk	6XY4	−8.1
Tumor necrosis factor receptor, TNFR	1NCF	−8.6
Tumor necrosis factor-related apoptosis-inducing ligand receptor, TRAIL	1D4V	−9.0
Apoptosis-mediating surface antigen FAS	3TJE	−8.5
FAS-associated death domain, FADD	3EZQ	−8.2
TNFR1-associated death domain protein, TRADD	1F3V	−7.4
Caspase-7	1K86	−10.3
Caspase-8	1I4E	−8.8
Tumor protein p53	4MZI	−8.2

Ferroptosis pathway

Molecular docking also revealed STM's strong association with other non-apoptotic cell death pathways. Ferroptosis involves lipid peroxidation by iron to achieve cell death, a phenomenon largely observed in pathophysiological conditions [76]. STM showed a significant interaction with the anti-ferroptotic protein FSP1/AIFM2, achieving binding affinity energy of −12.09 kcal/mol, as shown in **Table 6**. As FSP1 inhibits lipid peroxidation to prevent ferroptosis [77], thus, STM's strong binding indicates a possible modulatory role to diminish its function and induce cell death in ESCC cells.

Table 6 Binding affinity energies of STM resulted from the *in silico* molecular docking toward corresponding anti-ferroptotic proteins in ESCC.

Target Proteins **Anti-ferroptotic**	PDB Code	Binding Affinity Energy (kcal/mol)
Ferroptosis suppressor protein 1, FSP1 OR Apoptosis-Inducing Factor, Mitochondrion-Associated 2, AIFM2	8JSC	−12.1

Necroptosis pathway

Furthermore, STM was also targeting necroptosis to induce ESCC cell death. In circumstances where apoptosis is inhibited, cell death is achieved via necroptosis. Necroptosis is described as a regulated necrotic death that contributes to inflammation by releasing damage-associated molecular patterns (DAMPs) [78]. With binding affinities of −10.8 kcal/mol for MLKL and −10 kcal/mol for RIPK3 (**Table 7**), STM could possibly induce necroptosis in apoptosis-resistant cancer cells [79] by targeting these key proteins.

Table 7 Binding affinity energies of STM resulted from the *in silico* molecular docking toward corresponding necroptosis-related proteins in ESCC.

Target Proteins **Necroptosis-Related**	**PDB Code**	**Binding Affinity Energy (kcal/mol)**
Tumor necrosis factor alpha, TNFα	1A8M	−8.1
Receptor-interacting serine/threonine-protein kinase 1, RIPK1	4ITH	−7.9
Receptor-interacting serine/threonine-protein kinase 3, RIPK3	7MON	−10.0
Mixed lineage kinase domain like pseudokinase, MLKL	4M67	−10.8
Dynamin-related protein 1 (Drp1) OR dynamin-1-like protein (DNM1L)	3W6N	−9.4

Pyroptosis pathway

Similarly, STM shows strong association with pyroptosis, a pro-inflammatory lytic form of cell death [80], in **Table 8**. Strong predicted binding affinity was observed with pyroptosis-related proteins, notably with pyrin (−9.4 kcal/mol), followed by interleukin-1β (IL-1β) (−9.3 kcal/mol), Gasdermin D (GSDMD) (−8.3 kcal/mol), and caspase-1 (−7.5 kcal/mol) [81]. The potential influence of STM on the pyroptotic pathway may also contribute to tumor regression [82].

In summary, STM showed strong binding affinities with the selected target proteins, with the highest binding energy observed with pro-apoptotic APAF-1 (−12.3 kcal/mol), anti-ferroptotic FSP1/ AIFM2 (−12.09 kcal/mol), and anti-apoptotic Hsp70 (−11 kcal/mol), which are further observed their 2D and 3D topological interactions in **Figures 6** - **8**. These results collectively suggest that STM can modulate a wide array of proteins to induce cell death through multiple regulated pathways.

Table 8 Binding affinity energies of STM resulted from the *in silico* molecular docking toward corresponding pyroptosis-related proteins in ESCC.

Target Proteins **Pyroptosis-Related**	**PDB Code**	**Binding Affinity Energy (kcal/mol)**
Interferon-inducible protein, AIM2 (Absent in melanoma 2)	3RN2	−8.4
Pyrin	4CG4	−9.4
Caspase-1	2FQQ	−7.5
Gasdermin D, GSDMD	6N9O	−8.3
Interleukin IL-1β	1I1B	−9.3

Topology interactions of STM with target proteins

Furthermore, the exact interaction and binding between STM and amino acid residues in 2D and 3D topologies were also observed and compared. STM's predicted binding mechanism with Hsp70 involves non-covalent interactions with residues localized within the Nucleotide Binding Domain (NBD) (**Figure 6**). The receptor-ligand complex was driven by a network of polar and non-polar bonds, primarily the conventional hydrogen bonds with THR A:14, TYR A:15, and GLY A:202 (contact distance 6.0 Å), while supplementary

carbon-hydrogen bonds formed with THR A:13, TYR A:15, and SER A:340 (contact distance 4.6 Å). Remarkably, TYR A:15 contributed to both polar and non-polar stabilization through a pi-alkyl bond (contact distance 5.4 Å), anchoring the ligand within the binding pocket. These specific interactions were further reinforced by numerous van der Waals forces across a wide range of residues. Nonetheless, the stability of the predicted pose was slightly counteracted by unfavorable donor-donor interactions identified with GLY A:202 and GLY A:203 (contact distance 4.2 Å). This may indicate repulsive forces between the ligand and receptor, contributing potential instability to the receptor-ligand complex [83]. The NBD functions primarily to bind to ATP, allowing Hsp70 to adopt an 'open' conformation for exchange of client proteins, where hydrolysis of ATP will induce a conformational rearrangement to further stabilize the bound substrates [84]. By competing with ATP at the NBD, STM could block nucleotide binding or hinder hydrolysis, which forces Hsp70 to be in an inactive state, deteriorating its role to stabilize unfolded polypeptides and protect cancer cells under proteotoxic stress, leading to cancer cell death [85].

In the interaction with APAF-1 (**Figure 7**), STM's binding pose was stabilized through a network of conventional hydrogen bonds with residues GLY D:157, LYS D:160, SER D:161, ASP D:243, and ARG D:265 within the contact distance range of 4.2 Å. Weaker carbon-hydrogen bonds were formed with ASP D:243 and ASP D:392 (contact distance 5.6 Å), while hydrophobic interactions, including alkyl and pi-alkyl contacts, were established with ALA D:156, PHE D:425, TYR D:436, and HIS D:438 (contact distance of 6.4 Å). As visualized in the 3D interactions, the binding of STM is localized within the NB-ARC (nucleotide-binding adaptor shared by APAF-1, R proteins, and CED-4) domain, a conserved signaling motif that plays a critical role for ordinance of programmed cell death in animal cells [86]. Specifically, the NB subdomain functions as a catalytic side for ATP binding and hydrolysis [87], leading to conformational changes and oligomerization for the activation of apoptosomes [88]. Notably, STM was predicted to bind at the Walker A (P-loop) motif (GxxxxGKS/T), specifically interacting with GLY D:157, LYS D:160, SER D:161. As LYS D:160 normally coordinates the β- and γ-phosphates of ADP/ATP and SER D:161 contributes to Mg^{2+} ion binding [89], STM's predicted binding at these residues suggests a competitive inhibition of nucleotide association and hydrolysis. Such interference would be expected to diminish the oligomerization of APAF-1, leading to reduced apoptotic activities.

Similarly, STM's interactions with FSP1 were also based on non-covalent bonds, significantly within the N-terminal region and the FAD/NADH oxidoreductase domain, as shown in **Figure 8**. Conventional hydrogen bonds were formed with ASN C:248 and ASP C:285 (contact distance 4.75 Å), and carbon-hydrogen bonds with GLY C:20, ASP C:41, SER C:111, and ASP C:285 (contact distance 4.8 Å). Hydrophobic contacts were achieved with HIS C:47 and ALA C:298 (contact distance 7.05 Å). These specific interactions were further accompanied by van der Waals forces, which contribute to the overall stability of the receptor-ligand complex. Notably, several residues were located within the FAD-binding and NAD(P)H interaction pocket (ASN C:248, ASP C:285 and ALA C:298) [90], suggesting that STM is likely to compete with endogenous cofactors and substrates. These bindings could interfere with the enzymatic activity of FSP1, blocking the reduction of ubiquinone-10 to ubiquinol-10 with N-myristoylation and NAD(P)H as substrates [91]. This will disrupt the production of antioxidants from oxidized coenzyme Q10 (CoQ10) to produce antioxidants, promoting lipid peroxidation and therefore ferroptosis [92]. This potential ferroptosis-inducing role highlights the therapeutic advantage of STM, as it may selectively sensitize tumor cells, promoting efficiency of conventional therapies [93].

Overall, STM demonstrated favorable non-covalent interactions across Hsp70, APAF-1, and FSP1, with stability mediated primarily by hydrogen bonds, hydrophobic contacts, and van der Waals forces. In absence of covalent anchoring, STM's binding is suggested to be reversible [94], a property that may reduce off-target toxicity [95] but therapeutic efficacy would depend on maintaining a sufficiently high local concentration of STM for efficient competition with endogenous nucleotides or cofactors (ATP/ADP for Hsp70 and APAF-1 and NAD(P)H/FAD for FSP1) [96,97]. Moreover, the presence of unfavorable donor-donor interactions with Hsp70 and relatively loose hydrophobic contacts in FSP1 emphasizes areas where

binding stability could be improved. Future structural modifications to STM, such as incorporating substituents that enhance pi-pi stacking [98], create salt-bridge interactions [99], or reduce steric clashes [100] may potentially increase the binding stability and selectivity for better modulatory effects.

These *in silico* assessments suggest the possibilities of employing STM as a multi-target agent, a capability crucial for overcoming complex resistance mechanisms developed in cancerous cells [101].

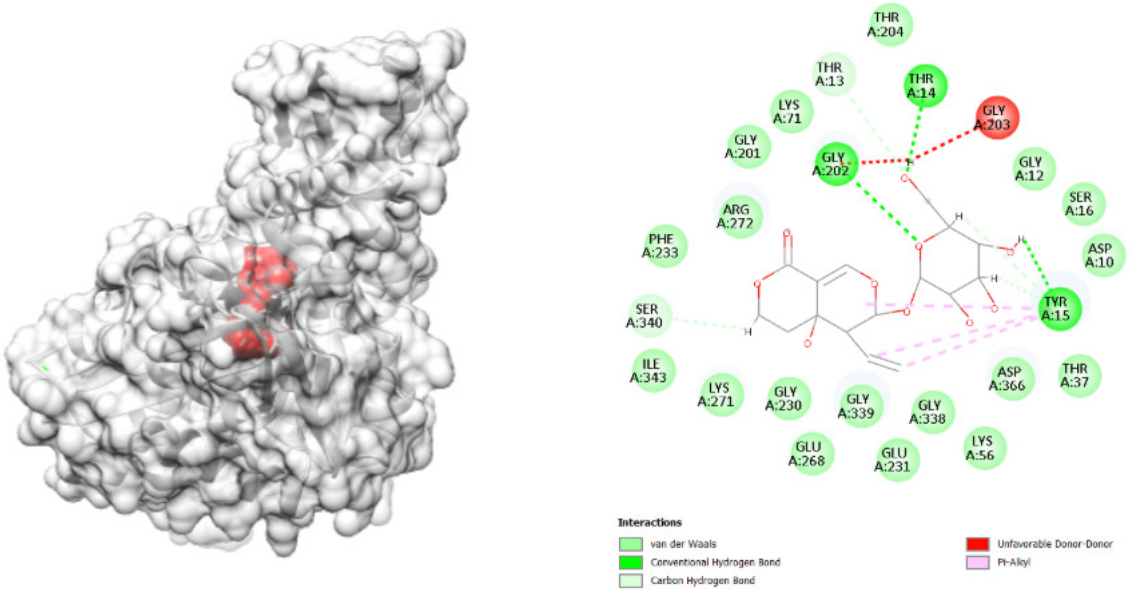


Figure 6 The binding of STM at the predicted active site of Hsp70 (x = 5.20, y = 14.82, z = 16.53) alongside the 2D topology interactions of STM with the residues of the binding pocket.

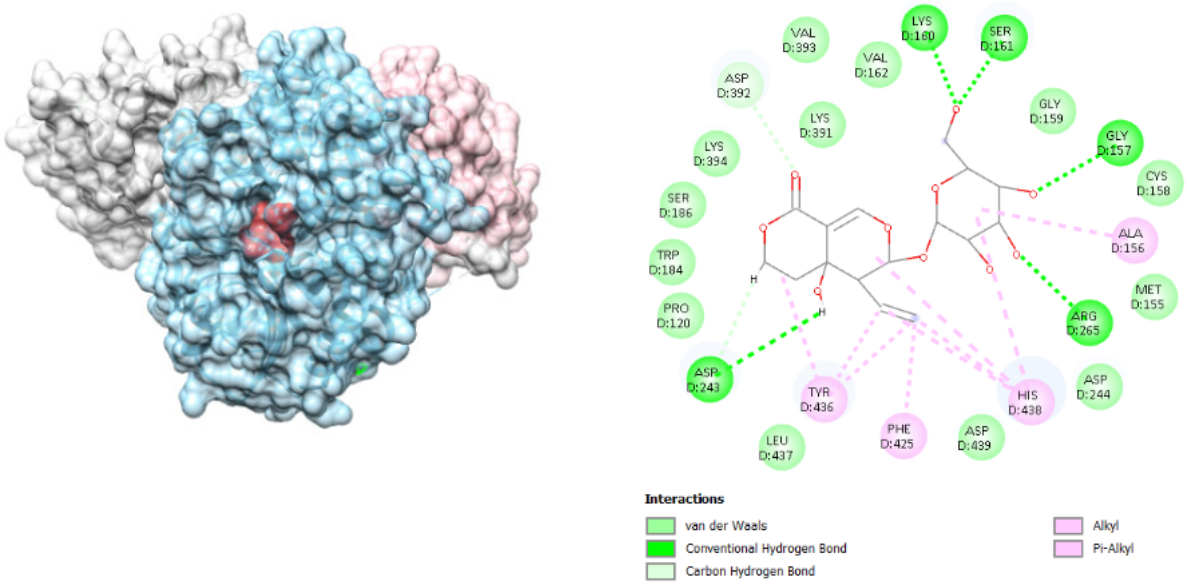


Figure 7 The binding of STM at the predicted active site of APAF-1 (x = 33.06, y = 76.43, z = 93.23) alongside the 2D topology interactions of STM with the residues of the binding pocket.

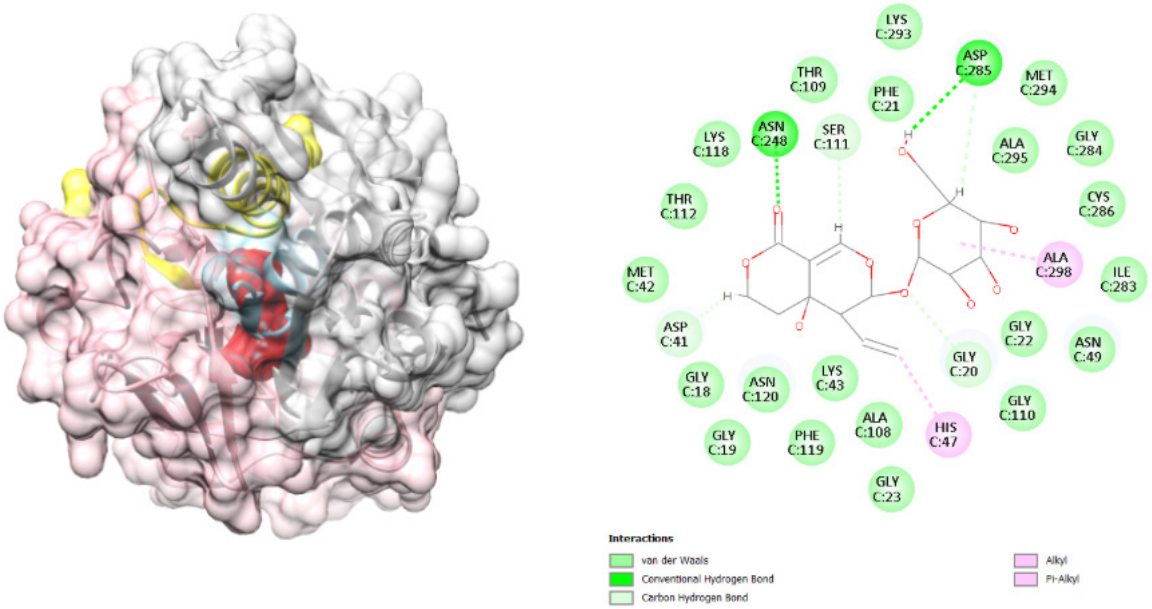


Figure 8 The binding of STM at the predicted active site of FSP1 (x= 13.63, y = 1.20, z = 9.24) and the 2D topology interactions of STM with the residues of the binding pocket.

Conclusions

This study provides strong *in vitro* evidence for the therapeutic potential of STM against ESCC cells. STM demonstrated a significant *in vitro* cytotoxicity against KYSE-150 cells (IC_{50} = 43.75 µM), showing favorable SI of 4.343 toward cancer cells over normal esophageal HET-1A cells (IC_{50} = 190 µM), which is greater than the SI = 0.668 of cisplatin. Besides, STM exhibited satisfactory drug-likeness and favorable ADMET profile, suggesting a reduced risk of systemic adverse effects. Moreover, the *in silico* molecular docking analysis further elucidated its potential as a multi-targeted agent to induce diverse cell death modalities, crucial to overcome drug resistance. To further validate the anticancer activity of STM against ESCC, more ESCC cell lines and predicted molecular mechanisms should also be confirmed using *in vitro* approach before testing in the *in vivo* model. Besides, the optimal drug delivery system for STM can be investigated to address challenges related to pharmacokinetic issues like limited oral bioavailability and potential toxicity. Overall, STM's promising profile deserves further investigation as a selective drug candidate for ESCC.

Acknowledgements

The authors gratefully acknowledge the support from the MAKNA Cancer Research Grant (GRTEX-OTR-DBS-MAKNA-2024-001), Sunway University Research Accelerator Grant Scheme (GRTIN-RAG-DBS-06-2026), and the final year project's financial aid from Sunway University, Malaysia.

CRediT author statement

Yuan Seng Wu: Conceptualization, Methodology, Software, Reviewing, Editing; **Fook Choy Yap**: Conceptualization, Methodology, Software, Reviewing, Editing, **Yan Mei Chong**: Investigation, Formal Analysis, Writing the Original Draft, Editing; **Bibi Ghausia Banon Aullyram**: Methodology, Investigation; **Sang Loon Tan**: Methodology; **Mahendran Sekar**: Methodology

References

[1] F Bray, M Laversanne, H Sung, J Ferlay, RL Siegel, I Soerjomataram and A Jemal. Global cancer statistics 2022: GLOBOCAN estimates of incidence and mortality worldwide for 36 cancers in 185 countries. *CA: A Cancer Journal for Clinicians* 2024; **74(3)**, 229-263.

[2] CQ Liu, YL Ma, Q Qin, PH Wang, Y Luo, PF Xu and Y Cui. Epidemiology of esophageal cancer in 2020 and projections to 2030 and 2040. *Thoracic Cancer* 2023; **14(1)**, 3-11.

[3] G Abbas and M Krasna. Overview of esophageal cancer. *Annals of Cardiothoracic Surgery* 2017; **6(2)**, 131.

[4] Z Fang, T Xia, S Pan, C Xu, S Ju, Z Shen and J Zhao. Esophageal carcinosarcoma comprising undifferentiated pleomorphic sarcoma and squamous cell carcinoma: A case report. *Journal of Cardiothoracic Surgery* 2022; **17(1)**, 210.

[5] A Ji, R Jin, R Zhang and H Li. Primary small cell carcinoma of the esophagus: Progression in the last decade. *Annals of Translational Medicine* 2020; **8(7)**, 502.

[6] J Qu, Y Zhuang, D Zheng, F Huang and S Zhang. Primary esophageal lymphoma: Clinical experience in diagnosis and treatment. *Cureus* 2021; **13(9)**, e17628.

[7] E Morgan, I Soerjomataram, H Rumgay, HG Coleman, AP Thrift, J Vignat, M Laversanne, J Ferlay and M Arnold. The global landscape of esophageal squamous cell carcinoma and esophageal adenocarcinoma incidence and mortality in 2020 and projections to 2040: New estimates from GLOBOCAN 2020. *Gastroenterology* 2022; **163(3)**, 649-658.

[8] G Businello, P Parente, L Mastracci, G Pennelli, G Traverso, M Milione, E Milione, M Michelotto, A Kotsafti, F Grillo and M Fassan. The pathologic and molecular landscape of esophageal squamous cell carcinogenesis. *Cancers* 2020; **12(8)**, 2160.

[9] M Sheikh, H Poustchi, A Pourshams, A Etemadi, F Islami, M Khoshnia, A Gharavi, M Hashemian, G Roshandel, H Khademi, M Zahedi, B Abedi-Ardekani, P Boffetta, F Kamangar, SM Dawsey, PD Pharaoh, CC Abnet, NE Day, P Brennan and R Malekzadeh. Individual and combined effects of environmental risk factors for esophageal cancer based on results from the Golestan cohort study. *Gastroenterology* 2019; **156(5)**, 1416-1427.

[10] H Simba, H Kuivaniemi, CC Abnet, G Tromp and V Sewram. Environmental and life-style risk factors for esophageal squamous cell carcinoma in Africa: A systematic review and meta-analysis. *BMC Public Health* 2023; **23(1)**, 1782.

[11] L Wang, YM Jia, J Zuo, YD Wang, ZS Fan, L Feng, X Zhang, J Han, WJ Lyu and ZY Ni. Gene mutations of esophageal squamous cell carcinoma based on next-generation sequencing. *Chinese Medical Journal* 2021; **134(6)**, 708-715.

[12] C Weidenbaum and MK Gibson. Approach to localized squamous cell cancer of the esophagus. *Current Treatment Options in Oncology* 2022; **23(10)**, 1370-1387.

[13] N Jiang, XL Ge, ZY Zhang, J Liu, PP Wang, XC Sun and M Yang. Prognostic factors for patients with esophageal cancer receiving definitive radiotherapy alone: A retrospective analysis. *Cancer Management and Research* 2021; **13**, 3229-3234.

[14] HC Puhr, GW Prager and A Ilhan-Mutlu. How we treat esophageal squamous cell carcinoma. *ESMO Open* 2023; **8(1)**, 100789.

[15] MC da Silva, LC Fabiano, KC da Costa Salomão, PLZ de Freitas, CQ Neves, SC Borges, MDG de Souza Carvalho, AC Breithaupt-Faloppa, AA de Thomaz, AM Dos Santos and NC Buttow. A rodent model of human-dose-equivalent 5-fluorouracil: Toxicity in the liver, kidneys, and lungs. *Antioxidants* 2023; **12(5)**, 1005.

[16] EA Elmorsy, S Saber, RS Hamad, MA Abdel-Reheim, AF El-kott, MA AlShehri, K Morsy, SA Salama and ME Youssef. Advances in understanding cisplatin-induced toxicity: Molecular mechanisms and protective strategies. *European Journal of Pharmaceutical Sciences* 2024; **203**, 106939.

[17] N Jose, A Joel, RJ Selvakumar, J Ramireddy, AO John, JT Georgy, A Singh and TS Ram. Diagnosis and management of 5-fluorouracil (5-fu)-induced acute leukoencephalopathy: Lessons learnt from a single-centre case series. *Journal of the Egyptian National Cancer Institute* 2022; **34(1)**, 22.

[18] S Shruthi and K Bhasker Shenoy. Cisplatin resistance in cancer therapy: Causes and overcoming strategies. *ChemistrySelect* 2024; **9(25)**, e202401449.

[19] Y Lugones, P Loren and LA Salazar. Cisplatin resistance: Genetic and epigenetic factors involved. *Biomolecules* 2022; **12(10)**, 1365.

[20] J Wonglhow, P Wetwittayakhlang, P Sunpaweravong, C Sathitruangsak and A

Dechaphunkul. Comparing the efficacy of carboplatin plus 5-fluorouracil, cisplatin plus 5-fluorouracil, and best supportive care for advanced esophageal squamous cell carcinoma: A propensity score analysis from a tertiary hospital in Southern Thailand. *Journal of Clinical Medicine* 2024; **13(6)**, 1735.

[21] NS Muhamad Fadzil, M Sekar, SH Gan, SR Bonam, YS Wu, J Vaijanathappa, S Ravi, PT Lum and SB Dhadde. Chemistry, pharmacology and therapeutic potential of swertiamarin - a promising natural lead for new drug discovery and development. *Drug Design, Development and Therapy* 2021; **15**, 2721-2746.

[22] X Wang and T Wang. Swertiamarin exerts anticancer effects on human cervical cancer cells via induction of apoptosis, inhibition of cell migration and targeting of MEK-ERK pathway. *Tropical Journal of Pharmaceutical Research* 2021; **20(1)**, 75-81.

[23] J Wu, Y Li, X Li and T Wu. Swertiamarin attenuates paraquat-induced pulmonary epithelial-like cell apoptosis via NOX4-mediated regulation of redox and mitochondrial function. *Brazilian Journal of Pharmaceutical Sciences* 2023; **59**, e22476.

[24] S Xiao, H Tang, Y Bai, R Zou, Z Ren, X Wu, Z Shi, S Lan, W Liu, T Wu, C Zhang and L Wang. Swertiamarin suppresses proliferation, migration, and invasion of hepatocellular carcinoma cells via negative regulation of FRAT1. *European Journal of Histochemistry* 2020; **64(4)**, 3169.

[25] L Li, S Xiao, X Dai, Z Tang, Y Wang, M Ali, FS Ataya, I Sahar, M Iqbal, Y Wu and K Li. Multi-omics analysis and the remedial effects of swertiamarin on hepatic injuries caused by CCl4. *Ecotoxicology and Environmental Safety* 2024; **282**, 116734.

[26] Q Zhang, K Chen, T Wu and H Song. Swertiamarin ameliorates carbon tetrachloride-induced hepatic apoptosis via blocking the PI3K/Akt pathway in rats. *The Korean Journal of Physiology & Pharmacology* 2019; **23(1)**, 21-28.

[27] Y Zhu, H Li, M Ma, D Li, O Zhang, S Cai, Y Wang, D Chen, S Jin, C Ding and L Xu. Swertiamarin ameliorates diet-induced obesity by promoting adipose tissue browning and oxidative metabolism in preexisting obese mice. *Acta Biochimica et Biophysica Sinica* 2022; **55(1)**, 131-142.

[28] HX Yang, YY Hu, R Liang, H Zheng and X Zhang. Progress in pharmacokinetics, pharmacological effects, and molecular mechanisms of swertiamarin: A comprehensive review. *Cells* 2025; **14(15)**, 1173.

[29] EF Pettersen, TD Goddard, CC Huang, GS Couch, DM Greenblatt, EC Meng and TE Ferrin. UCSF Chimera-A visualization system for exploratory research and analysis. *Journal of Computational Chemistry* 2004; **25(13)**, 1605-1612.

[30] BIOVIA, Dassault systems, Available at: https://www.3ds.com/products/biovia/all-products, accessed July 2025.

[31] H Tang, Y Ke, Z Ren, X Lei, S Xiao, T Bao, Z Shi, R Zou, T Wu, J Zhou, CA Geng, L Wang and J Chen. Bioinformatics analysis of differentially expressed genes in hepatocellular carcinoma cells exposed to Swertiamarin. *Journal of Cancer* 2019; **10(26)**, 6526-6534.

[32] L Deng, X Wu, X Zhu, Z Yu, Z Liu, J Wang and Y Zheng. Combination effect of curcumin with docetaxel on the PI3K/AKT/mTOR pathway to induce autophagy and apoptosis in esophageal squamous cell carcinoma. *American Journal of Translational Research* 2021; **13(1)**, 57-72.

[33] C Fang, L Wu, X Yang, K Xie, P Zhang, Y Feng, H Ma and X Tong. Decursin suppresses esophageal squamous cell carcinoma progression via orchestrated cell cycle deceleration, apoptotic activation, and oncoprotein degradation. *International Journal of Molecular Sciences* 2025; **26(11)**, 5391.

[34] S Jiang, Y Qiu, Z Wang, Y Ji, X Zhang, X Yan and Z Zhan. Carnosic acid induces antiproliferation and anti-metastatic property of esophageal cancer cells via MAPK signaling pathways. *Journal of Oncology* 2021; **2021**, 4451533.

[35] Y Cui, W Huang, F Du, X Yin, L Feng and B Li. Therapeutic benefits of niraparib tosylate as radio sensitizer in esophageal squamous cell carcinoma: An *in vivo* and *in vitro* preclinical study. *Clinical and Translational Oncology* 2022; **24**, 1643-1656.

[36] T Minegaki, K Takara, R Hamaguchi, M Tsujimoto and K Nishiguchi. Factors affecting the sensitivity of human-derived esophageal carcinoma cell lines to 5-fluorouracil and cisplatin. *Oncology Letters* 2013; **5(2)**, 427-434.

[37] F Xue, H Yang, P Xu, S Zhang, N Britzen-Laurent, LL Bao, R Grützmann, C Krautz and C Pilarsky. CRISPR/Cas9 Screening Highlights PFKFB3 Gene as a Major Contributor to 5-Fluorouracil Resistance in Esophageal Cancer. *Cancers* 2025; **17(10)**, 1637.

[38] C Zhang, CL Luo, GS Shang, DX Jiang and Q Song. Galangin enhances anticancer efficacy of 5-fluorouracil in esophageal cancer cells and xenografts through NLR family pyrin domain containing 3 (NLRP3) downregulation. *Medical Science Monitor: International Medical Journal of Experimental and Clinical Research* 2021; **27**, e931630-1.

[39] DS Mahdi, RH Al Mosawi and KN Madlum. Evaluation of the effect of valproic acid on 5-fluorouracil cytotoxicity on colon cancer cells. An *in vitro* study. *Medical Journal of Ahl al-Bayt University* 2024; **3(1)**, 140-153.

[40] M Capula, C Corno, B El Hassouni, G Li Petri, S Aranđelović and EORTC PAMM Group. A brief guide to performing pharmacological studies *in vitro*: Reflections from the EORTC-PAMM course "Preclinical and Early-phase Clinical Pharmacology." *Anticancer Research* 2019; **39(7)**, 3413-3418.

[41] A Moldasheva, L Bakyt, D Bulanin and M Aljofan. The impact of cellular environment on in vitro drug screening. *Future Science OA* 2023; **9(9)**, FSO900.

[42] CP Segeritz and L Vallier. *Cell culture: Growing cells as model systems in vitro. In*: M Jalali, FYL Saldanha and M Jalali (Eds.). Basic science methods for clinical researchers. Academic Press, San Diego, United States, 2017, p. 151-172.

[43] S Weiskirchen, SK Schröder, EM Buhl and R Weiskirchen. A beginner's guide to cell culture: Practical advice for preventing needless problems. *Cells* 2023; **12(5)**, 682.

[44] YS Wu, NS Rahim, A Stephen, SM Shin, NM Hashim, SCB Gopinath and HA Mahendran. Downregulation of transmembrane 4 superfamily 1 gene expression inhibits esophageal squamous cell carcinoma cell viability and Cisplatin resistance and regulates microRNA expression. *Medical Journal of Malaysia* 2024; **79**, 27.

[45] M Muralisankar, JR Chen, J Haribabu and SC Ke. Effective and selective Ru(II)-arene complexes containing 4,4′-substituted 2,2′-bipyridine ligands targeting human urinary bladder cancer cells. *International Journal of Molecular Sciences* 2023; **24(15)**, 11896.

[46] C Zhang, C Xu, X Gao and Q Yao. Platinum-based drugs for cancer therapy and anti-tumor strategies. *Theranostics* 2022; **12(5)**, 2115-2132.

[47] J Lee, JL Beers, RM Geffert and KD Jackson. A review of CYP-mediated drug interactions: Mechanisms and *in vitro* drug-drug interaction assessment. *Biomolecules* 2024; **14(1)**, 99.

[48] TK Karami, S Hailu, S Feng, R Graham and HJ Gukasyan. Eyes on Lipinski's rule of five: A new "rule of thumb" for physicochemical design space of ophthalmic drugs. *Journal of Ocular Pharmacology and Therapeutics* 2022; **38(1)**, 43-55.

[49] S Bashiardes and C Christodoulou. Orally administered drugs and their complicated relationship with our gastrointestinal tract. *Microorganisms* 2024; **12(2)**, 242.

[50] CA Lipinski, F Lombardo, BW Dominy and PJ Feeney. Experimental and computational approaches to estimate solubility and permeability in drug discovery and development settings. *Advanced Drug Delivery Reviews* 2001; **46(1-3)**, 3-26.

[51] DF Veber, SR Johnson, HY Cheng, BR Smith, KW Ward and KD Kopple. Molecular properties that influence the oral bioavailability of drug candidates. *Journal of Medicinal Chemistry* 2002; **45(12)**, 2615-2623.

[52] WJ Egan, KM Merz and JJ Baldwin. Prediction of drug absorption using multivariate statistics. *Journal of Medicinal Chemistry* 2000; **43(21)**, 3867-3877.

[53] I Muegge, SL Heald and D Brittelli. Simple selection criteria for drug-like chemical matter. *Journal of Medicinal Chemistry* 2001; **44(12)**, 1841-1846.

[54] O Afzal, ASA Altamimi, MS Nadeem, SI Alzarea, WH Almalki, A Tariq, B Mubeen, BN Murtaza, S Iftikhar, N Riaz and I Kazmi. Nanoparticles in drug delivery: From history to therapeutic applications. *Nanomaterials* 2022; **12(24)**, 4494.

[55] TC Ezike, US Okpala, UL Onoja, PC Nwike, EC Ezeako, JO Okpara, CC Okoroafor, SC Eze, OL Kalu, EC Odoh, U Nwadike, JO Ogbodo, BU Umeh, EC Ossai and BC Nwanguma. Advances in drug delivery systems, challenges and future directions. *Heliyon* 2023; **9(6)**, e17488.

[56] F Laffleur, G Millotti and J Lagast. An overview of oral bioavailability enhancement through self-emulsifying drug delivery systems. *Expert Opinion on Drug Delivery* 2025; **22(5)**, 659-671.

[57] C Winder, R Azzi and D Wagner. The development of the globally harmonized system (GHS) of classification and labelling of hazardous chemicals. *Journal of Hazardous Materials* 2005; **125(1-3)**, 29-44.

[58] TA Loomis and AW Hayes. *Toxicologic testing methods*. *In*: AW Hayes and TA Loomis (Eds.). Loomis's essentials of toxicology. 4th ed. Academic Press, San Diego, United States, 1996, p. 205-248.

[59] F Rivero-Pino, MC Millan-Linares and S Montserrat-de-la-Paz. Strengths and limitations of *in silico* tools to assess physicochemical properties, bioactivity, and bioavailability of food-derived peptides. *Trends in Food Science & Technology* 2023; **138**, 433-440.

[60] P Banerjee, E Kemmler, M Dunkel and R Preissner. ProTox 3.0: A webserver for the prediction of toxicity of chemicals. *Nucleic Acids Res* 2024; **52(W1)**, W513-W520.

[61] A Daina, O Michielin and V Zoete. SwissADME: A free web tool to evaluate pharmacokinetics, drug-likeness and medicinal chemistry friendliness of small molecules. *Scientific Reports* 2017; **7(1)**, 42717.

[62] J Lica, M Wieczór, GJ Grabe, MW Jancz, M Misiak, K Gucwa, W Brankiewicz, N Maciejewska, A Stupak, M Baginski, K Rolka, A Hellmann and AC Skladanowski. Effective drug concentration and selectivity depends on fraction of primitive cells. *International Journal of Molecular Sciences* 2021; **22(9)**, 4931.

[63] MA Mahmood, AH Abd and EJ Kadhim. Assessing the cytotoxicity of phenolic and terpene fractions extracted from Iraqi Prunus arabica against AMJ13 and SK-GT-4 human cancer cell lines. *F1000Research* 2024; **12**, 433.

[64] MJ Goldstein, M Peters, BL Weber and CB Davis. Optimizing the Therapeutic Window of Targeted Drugs in Oncology: Potency-Guided First-in-Human Studies. *Clinical and Translational Science* 2021; **14(2)**, 536-543.

[65] Z Yang, R Ma, J Li and L Zhao. Noncoding RNAs in esophageal cancer: A glimpse into implications for therapy resistance. *Pharmacological Research* 2023; **188**, 106678.

[66] S Ghafouri-Fard, A Abak, F Tondro Anamag, H Shoorei, F Fattahi, SA Javadinia, A Basiri and M Taheri. 5-Fluorouracil: A narrative review on the role of regulatory mechanisms in driving resistance to this chemotherapeutic agent. *Frontiers in Oncology* 2021; **11**, 658636.

[67] M Barathan, AK Zulpa, SL Ng, Y Lokanathan, MH Ng and JX Law. Innovative strategies to combat 5-Fluorouracil resistance in colorectal cancer: The role of phytochemicals and extracellular vesicles. *International Journal of Molecular Sciences* 2024; **25(13)**, 7470.

[68] A Dutta, A Chakraborty, T Ghosh and A Kumar. 5-Fluorouracil induces apoptosis in nutritional deprived hepatocellular carcinoma through mitochondrial damage. *Scientific Reports* 2024; **14(1)**, 23387.

[69] F Ramos-Martin and N D'Amelio. Drug Resistance: An Incessant Fight against Evolutionary Strategies of Survival. *Microbiology Research* 2023; **14(2)**, 507-542.

[70] O Morana, W Wood and CD Gregory. The apoptosis paradox in cancer. *International Journal of Molecular Sciences* 2022; **23(3)**, 1328.

[71] M Mustafa, R Ahmad, IQ Tantry, W Ahmad, S Siddiqui, M Alam, K Abbas, Moinuddin, MI Hassan, S Habib and S Islam. Apoptosis: A comprehensive overview of signaling pathways, morphological changes, and physiological significance and therapeutic implications. *Cells* 2024; **13(22)**, 1838.

[72] KD Kaloni, ST Diepstraten, A Strasser and GL Kelly. BCL-2 protein family: Attractive targets for cancer therapy. *Apoptosis* 2023; **28(1)**, 20-38.

[73] C Hu, J Yang, Z Qi, H Wu, B Wang, F Zou, H Mei, J Liu, W Wang and Q Liu. Heat shock proteins: Biological functions, pathological roles, and therapeutic opportunities. *MedComm* 2022; **3(3)**, e161.

[74] J Ruan, X Wei, S Li, Z Ye, L Hu, R Zhuang, Y Cao, S Wang, S Wu, D Peng, S Chen, S Yuan and A Xu. Apaf-1 is an evolutionarily conserved DNA sensor that switches the cell fate between apoptosis and inflammation. *Cell Discovery* 2025; **11(1)**, 4.

[75] G Sahoo, D Samal, P Khandayataray and MK Murthy. A review on caspases: Key regulators of biological activities and apoptosis. *Molecular Neurobiology* 2023; **60(10)**, 5805-5837.

[76] J Li, F Cao, H Yin, Z Huang, Z Lin, N Mao, B Sun and G Wang. Ferroptosis: Past, present and future. *Cell Death & Disease* 2020; **11(2)**, 88.

[77] TN Xavier da Silva, C Schulte, AN Alves, HM Maric and JP Friedmann Angeli. Molecular characterization of AIFM2/FSP1 inhibition by iFSP1-like molecules. *Cell Death & Disease* 2023; **14(4)**, 281.

[78] X Liu, X Xie, Y Ren, Z Shao, N Zhang, L Li, X Ding and L Zhang. The role of necroptosis in disease and treatment. *MedComm* 2021; **2(4)**, 730-755.

[79] YK Dhuriya and D Sharma. Necroptosis: A regulated inflammatory mode of cell death. *Journal of Neuroinflammation* 2018; **15(1)**, 199.

[80] Z Rao, Y Zhu, P Yang, Z Chen, Y Xia, C Qiao, W Liu, H Deng, J Li, P Ning and Z Wang. Pyroptosis in inflammatory diseases and cancer. *Theranostics* 2022; **12(9)**, 4310-4329.

[81] P Broz. Pyroptosis: Molecular mechanisms and roles in disease. *Cell Research* 2025; **35(5)**, 334-344..

[82] R Loveless, R Bloomquist and Y Teng. Pyroptosis at the forefront of anticancer immunity. *Journal of Experimental & Clinical Cancer Research* 2021; **40(1)**, 264.

[83] HA Odhar, AF Hashim and SS Humad. Molecular docking analysis and dynamics simulation of salbutamol with the monoamine oxidase B (MAO-B) enzyme. *Bioinformation* 2022; **18(3)**, 304-309.

[84] MP Mayer and LM Gierasch. Recent advances in the structural and mechanistic aspects of Hsp70 molecular chaperones. *The Journal of Biological Chemistry* 2019; **294(6)**, 2085-2097.

[85] MK Singh, S Han, S Ju, JS Ranbhise, J Ha, SG Yeo, SS Kim and I Kang. Hsp70: A Multifunctional Chaperone in Maintaining Proteostasis and Its Implications in Human Disease. *Cells* 2025; **14(7)**, 509.

[86] Y Wang, Z Teng, H Li, W Wang, F Xu, K Sun, J Chu, Y Qian, GJ Loake, C Chu and J Tang. An activated form of NB-ARC protein RLS1 functions with cysteine-rich receptor-like protein RMC to trigger cell death in rice. *Plant Communications* 2023; **4(2)**, 100459.

[87] G van Ooijen, G Mayr, MMA Kasiem, M Albrecht, BJC Cornelissen and FLW Takken. Structure-function analysis of the NB-ARC domain of plant disease resistance proteins. *Journal of Experimental Botany* 2008; **59(6)**, 1383-1397.

[88] N Maruta, H Burdett, B Lim, X Hu, S Desa, MK Manik and B Kobe. Structural basis of NLR activation and innate immune signalling in plants. *Immunogenetics* 2022; **74(1)**, 5-26.

[89] WIL Tameling, JH Vossen, M Albrecht, T Lengauer, JA Berden, MA Haring, BJC Cornelissen and FLW Takken. Mutations in the NB-ARC domain of I-2 that impair ATP hydrolysis cause autoactivation. *Plant Physiology* 2006; **140(4)**, 1233-1245.

[90] W Li, L Liang, S Liu, H Yi and Y Zhou. FSP1: A key regulator of ferroptosis. *Trends in Molecular Medicine* 2023; **29(9)**, 753-764.

[91] J Lee and JL Roh. Unleashing ferroptosis in human cancers: Targeting ferroptosis suppressor protein 1 for overcoming therapy resistance. *Antioxidants* 2023; **12(6)**, 1218.

[92] S Feng, X Huang, D Tang, X Liu, L Ouyang, D Yang, K Wang, B Liao and S Qi. The crystal structure of human ferroptosis suppressive protein 1 in complex with flavin adenine dinucleotide and nicotinamide adenine nucleotide. *MedComm* 2024; **5(3)**, e479.

[93] Z Jin, Q Zhang, Y Pan, H Chen, K Zhou, H Cai and P Huang. Roles and prospective applications of ferroptosis suppressor protein 1 (FSP1) in malignant tumor treatment. *Current Oncology* 2025; **32(8)**, 456.

[94] Y Liu, L Si, Y Jiang, S Jiang, X Zhang, S Li, J Chen and J Hu. Design of pH-responsive nanomaterials based on the tumor microenvironment. *International Journal of Nanomedicine* 025; **20(0)**, 705-721.

[95] Faridoon, R Ng, G Zhang and JJ Li. An update on the discovery and development of reversible covalent inhibitors. *Medicinal Chemistry Research* 2023; **32(6)**, 1039-1062.

[96] DS Johnson, E Weerapana and BF Cravatt. Strategies for discovering and derisking covalent, irreversible enzyme inhibitors. *Future Medicinal Chemistry* 2010; **2(6)**, 949-964.

[97] B Lubinski and GR Whittaker. Host cell proteases involved in human respiratory viral infections and their inhibitors: A review. *Viruses* 2024; **16(6)**, 984.

[98] KK Kumaree, NVA Anthikapalli and A Prasansuklab. *In silico* screening for potential inhibitors from the phytocompounds of Carica papaya against Zika virus NS5 protein. *F1000Research* 2024; **12**, 655.

[99] R Kurczab, P Śliwa, K Rataj, R Kafel and AJ Bojarski. Salt bridge in ligand-protein complexes - systematic theoretical and statistical investigations. *Journal of Chemical Information and Modeling* 2018; **58(11)**, 2224-2238.

[100] K Mierzejewska, M Bochtler and H Czapinska. On the role of steric clashes in methylation control of restriction endonuclease activity. *Nucleic Acids Research* 2016; **44(1)**, 485-495.

[101] P Garg, J Malhotra, P Kulkarni, D Horne, R Salgia and SS Singhal. Emerging therapeutic strategies to overcome drug resistance in cancer cells. *Cancers* 2024; **16(13)**, 2478.